Supplementary Information Appendix for

Targeted Inhibition of Gut Bacterial ß-glucuronidase Activity Enhances Anticancer Drug Efficacy

AUTHORS:

Aadra P. Bhatt, Samuel J. Pellock, Kristen A. Biernat, William G. Walton, Bret D. Wallace, Benjamin C. Creekmore, Marine M. Letertre, Jonathan R. Swann, Ian D. Wilson, Jose R. Roques, David B. Darr, Sean T. Bailey, Stephanie A. Montgomery, Jeffrey M. Roach, M. Andrea Azcarate-Peril, R. Balfour Sartor, Raad Z. Gharaibeh, Scott J. Bultman, and Matthew R. Redinbo

Corresponding Author: Matthew R. Redinbo
Email: redinbo@unc.edu

This PDF file includes:

www.pnas.org/cgi/doi/10.1073/pnas.1918095117

SUPPLEMENTARY MATERIALS AND METHODS

PROTEIN PURIFICATION, CRYSTALLIZATION, AND STRUCTURE DETERMINATION.

The *C. perfringens* GUS (*Cp*GUS) enzyme was expressed and purified as previously described (1). The *Cp*GUS was pre-incubated with 1 mM **UNC10201652** (see below) for 1 hour prior to co-crystallization setup. Co-crystals of *Cp*GUS-Inh9 were grown at 16 °C in 0.1 M 2-(*N*- amorpholino)ethanesulfonic acid (pH 6.0–6.5) and 28%–36% PEG 400. Crystals were flash-frozen in liquid nitrogen in preparation for X-ray data collection. Diffraction data were collected on the 23-ID beamline at GM/CA-CAT (Advanced Photon Source, Argonne National Laboratory). Data were indexed, scaled, and processed using standard methods(1) and the structure determined by molecular replacement with Phaser(2) using the apo-*Cp*GUS structure as a search model (PDB: 4JKM). Structure refinement was carried out using the automated Phenix refinement software package followed by manual structure refinement in COOT (3). The Inh-9 ligand file was generated using eLBOW (4) from the Phenix software suite and placed in electron density using the ligand search function of Coot. Coordinates and structure factors can be found at PDB: 6CXS. The data collection and refinement statistics are detailed in **Table S1**.

INHIBITORS

4-(8-(piperazin-1-yl)-1,2,3,4-tetrahydro-[1,2,3]triazino[4',5':4,5]thieno[2,3-c]isoquinolin-5- yl)morpholine, also known as UNC10201652, was synthesized in-house at the UNC Center for Integrative Chemical Biology and Drug Discovery (CICBDD) as previously reported (5). Inhibitor 1 was previously described (1).

ß-GLUCURONIDASE ACTIVITY ASSAYS

We employed a fluorometric assay to measure processing of SN38-G, which emits strong fluorescence at 420 nm when excited at 230 nm; fluorescence is lost upon hydrolysis of SN38-G to SN38. All reactions were carried out at 37 °C in black 96-well plates, and fluorescence was monitored using a Tecan Infinite Pro plate reader. ***In vitro* assays** contained 5 µL of purified enzyme, 5 µL of 10x buffer (250 mM HEPES, 250 mM NaCl, variable pH), 5 µL SN38-G (final concentration of 15 µM), and 35 µL of water. For *in vitro* inhibition assays,

conditions were the same except 5 µL of inhibitor (100 µM final) and 30 µL of water were added. Buffer, substrate, and inhibitor were pre-incubated for 10 minutes at 37 °C and the reaction was initiated by the addition of enzyme. For **bacterial *in cell* assays**, WT and GUSΔ413-504 *E. coli* K-12 MG1655 were grown overnight in 10 mL lysogeny broth (LB) in ambient air with shaking. The next morning, 20 µL of each was sub-cultured into 2 mL of fresh LB for one hour, after which 1 mM of 4-Nitrophenyl-ß-D-glucuronidase (PNPG) was added for one hour to induce expression of ß-glucuronidase; 10 µM inhibitor or equal volume DMSO was added to the cells at the same time (6). Each culture was grown to an optical density of approximately 0.6, after which bacteria were pelleted by centrifugation, washed 2x with LB containing 63 µg/mL chloramphenicol, and cells were lysed with 0.1% sodium dodecyl sulfate and chloroform with vigorous vortexing. 10 µL of resultant supernatant was used to initiate the hydrolysis reaction of 150 µM SN38- G in a reaction buffer comprised of 20mM HEPES, 50 mM NaCl at pH 7.4. For in cell inhibition assays, 10 µM of either Inh1 or UNC10201652 were used, with equal volume DMSO as control. For ***in fimo* assays** (7), frozen fecal samples were rehydrated in 15× assay buffer (weight/volume; 20 mM HEPES, 50 mM NaCl, pH 7.4, 1×*Complete*® Protease inhibitor cocktail [Roche]). Bacterial cells were lysed using a Tissuelyzer II (Qiagen) for two minutes at 30 Hertz. Homogenate was sonicated for four minutes, and then clarified by centrifugation for five minutes at *13,000* × *g*. All experimental manipulation until this point occurred at 4°C. 5 µL of fecal slurry supernatant was used to initiate the hydrolysis reaction of 150 µM SN38-G (or 500 µM of the non-specific GUS substrate 4-Methylumbelliferyl-β-D-glucuronide (4-MUG) in Figure S3C) resuspended in the same buffer. For all assays, reactions containing only SN38-G (or 4-MUG) or only buffer/bacterial lysate/fecal slurry were used as negative controls; a subset of samples were heat inactivated at 95°C for further background establishment. Each sample was assayed using three technical replicates, and each experiment was performed with a minimum of three biological replicates.

The initial velocities of the resultant progress curves of the reaction were calculated in MATLAB by linear regression. Initial velocities were then normalized to the protein concentration (*in vitro* assay), culture optical density (*in cell* assay) or total fecal protein content (*in fimo* assay) calculated using a standard Bradford assay. Fluorescence units were converted to concentration by standard curve analysis to generate the final units

presented. All statistical analysis was performed on Prism (Graphpad). Statistical tests are indicated in figure legends, and details on the analyses are reported in Table S6.

QUANTIFICATION OF GUSi AND IRINOTECAN METABOLITES

Sample preparation: Intestinal contents were thawed and homogenized just prior to weighing 50mg (+/- 0.5mg). Once vortex-mixed with ~100µL of Zirconium beads and 1.2mL of cold H_2O:Acetonitrile (2:1), two cycles of bead beating using the Percellys bead beater (6,500Hz, 40sec) were performed. The samples were centrifuged for 20 minutes (*17,000 x g* at 4℃), and the supernatants were distributed as follows: 250 µL for the first experimental replicate, 250 µL for the second and 500 µL for a pooled quality control (QC). Concentration under nitrogen flow of each replicate and the QCs were made in 3 hours. Re-suspension of the samples was done using 120 µL of H_2O:Acetonitrile (1:1) followed by a centrifugation during 5 minutes at *21,200 x g*. The supernatants were finally transferred into 350 µL volume 96-well-plates before placing into the UPLC sample manager. Plasma samples were thawed and vortex mixed with cold Acetonitrile:Methanol (2:1) according the proportion 1:3 (v/v) before placing at -20℃ overnight. The samples were centrifuged 10 minutes at *17,000 x g* at 4℃ prior the collection of the supernatants and their concentration under nitrogen flow overnight. The samples were then dissolved into 120 µL of H_2O:Acetonitrile (1:1), centrifuged for 5 minutes at *21,200 x g* and finally 100 µL was transferred into a well-plate and 20 µL to a pool QC.

Standards: 2mg/mL GUSi-UNC10201652 stock solution was prepared in DMSO. Intermediate solutions were prepared at 2.5 µg/mL using H_2O:Acetonitrile (1:1) to dilute. Calibration curves (5 – 20 – 40 – 80 – 120 – 240 – 320 – 420 – 560 – 640 – 720 – 820 – 1000 ng/mL), and QCs (15 – 400 – 800 ng/mL) were prepared using these, and all solutions were kept at 4℃.

Targeted UPLC-MS: UPLC-MS was carried out on the ACQUITY UPLC-MS system using the Waters Xevo TQ-S mass spectrometer. The column used was an ACQUITY UPLC CSH C18 column (1,7µm, 2.1 x 50mm, 130Å). The solvents used were H_20 0.1% formic acid for A and ACN 0.1% formic acid for B. The gradient was cut shorter and initially as followed: starting with 5% B during the 1^{st} minute, reaching a plateau at 70% of B from 6 to 8 minutes, before it reaches 90% of B from 8.5 to 10 minutes and finally re-equilibrates from 10.10 to 12 minutes with 5% of B. A shallowed gradient was created: starting with 5% B during the 1^{st} minute, reaching

20% of B at 2 minutes, 35% at 4.5 minutes and 70% of B from 6.5 to 8 minutes, the end staying un-changed. Partial-loop with needle-overfill was the mode of injection selected and the volume injected was fixed at 6 µL.

The Waters Xevo TQ-S was used in positive electrospray ionization mode. The desolvation temperature was set at 550℃, the source temperature at 120℃, the capillary voltage at 5kV and the cone gas flow at 150 L/hour. The 412.0 → 384.1 monitor reaction monitoring (MRM) transition was selected for GUSi. The data were acquired and analysed using MassLynx and TargetLynx V4.1 (Waters), respectively.

ANIMAL STUDY DESIGNS

All animal studies were approved by the University of North Carolina Institutional Animal Care and Use Committee (IACUC), according to Care and Use of Laboratory Animals guidelines set by the National Institutes of Health. Mice were housed 2-3 per cage, and 3-4 cages were used for each treatment group. Given that breast cancer primarily afflicts females, female mice were chosen for all experiments. All animals (except for germ-free mice used in monoassociation studies described below) were maintained in specific-pathogen free (SPF) conditions in sterile micro-ventilator cages containing corn bedding. All animals were given free access to chow and water, both of which were sterilized for the athymic mice that were housed in sterilized cages.

Drugs were administered between one and two hours after the start of light cycle, to control for irinotecan chronotoxicity (circadian effects of irinotecan (8). Mice received GUSi or vehicle by twice daily oral gavage (10 µg in the morning and evening for GUSi, or vehicle) to remain consistent with mouse dosing schedules employed previously with Inh 1 and related chemotypes(9, 10). All animals were closely monitored for moribund signs, and were regularly weighed; animals were euthanized if they lost 20% body weight. Prior to terminal dissections, animals were deeply anesthetized using ketamine-xylazine, and cardiac puncture was used to collect blood. Plasma was separated from the remainder blood using Li-EDTA followed by centrifugation.

Spleens and tumors were dissected using sterile instruments, weighed and preserved in 10% neutral buffered formalin (NBF). Colon swiss rolls were prepared as previously described (11) and similarly preserved. Colon luminal contents were collected in sterile microfuge tubes, snap frozen and stored at -80°C until functional

enzyme assays and/or metataxonomic analyses were carried out. Transverse sections of the anterior duodenum, geometric midpoint of small intestine, and ileocecal junction (3-5 mm of each) were placed in mesh histocassettes and also preserved in 10% NBF. All tissues were fixed for 48h, extensively washed, embedded in paraffin, and 5 µm sections were prepared. Hematoxylin and eosin staining was performed per routine protocols. Immunohistochemical detection of BrdU was performed using standard protocols (12), with antigen retrieval at 95°C for 20 min in 10 mM sodium citrate (pH 6.0) and 0.05% (vol/vol) Tween 20. Anti- BrdU antibody was purchased from Abcam (AB 6326). After slides were stained with DAB (or NovaRed® for Figure S3F), counterstained with hematoxylin, cleared and mounted, images were acquired using an Olympus BX61 upright wide field microscope equipped with Volocity Imaging software. Figures were prepared using NIH Image J and Adobe Photoshop.

A. XENOGRAFT STUDIES

Sum149 (*BRCA1*-mutant) cell line, a representative basal-like breast cancer cell line, was obtained from the ATCC. Cells were cultured in fully-supplemented HuMEC media (Gibco) with additional antibiotic-antimycotic (Gibco), and maintained at 37°C with 5% CO2. 2 x 10^6 freshly harvested cells were suspended in matrigel and subcutaneously injected into the left flank of female athymic nude mice bred in-house at UNC. Mice were 10 weeks old, with a minimum weight of 20 g. Mice were regularly monitored for tumor formation, and once tumors were palpable (~100 mm^3) mice were randomized into one of four groups: control, GUSi, Irinotecan, Irinotecan + GUSi, and treatment was initiated. Tumors were measured using the formula (Length x $Width^2$)/2. Dosing details are tabulated in Table S2. Animals were closely monitored for diarrhea, and their weights were measured regularly; animals losing >20% body weight were euthanized.

B. C3-TAG TRANSGENIC MICE

FVB-TG(C3-1-TAG)cJeg/JegJ, referred here as C3TAg mice used in Figure 4 are previously described (13, 14). In this model, the C3(1) component of the prostate steroid binding protein (PSBP) targets expression of the SV40 polyoma virus Large T Antigen (Tag) to the murine mammary epithelium, resulting in tumors that histologically resemble human disease. Therefore, because this model is T antigen-driven, tumor incidence is

uniform in all animals irrespective of experimental therapy. Atypia begins in young animals (8 weeks), and by 12 weeks of age develops into intraepithelial neoplasia with features resembling human ductal carcinoma *in situ.* Fully invasive carcinomas arise at ~16 weeks in 100% of all female mice. Transgenic mice are screened *via* qPCR, in a Taq-Man assay using the Life Technologies QuantStudio 6. Primers and probes are listed in Table S5, and Figure S5. qPCR conditions: 95°C for 10 minutes, followed by 40 cycles of 95° 15 seconds, 60° 1 minute. Treatment was initiated the same day that palpable masses were detected after randomization into one of four groups: control, GUSi, Irinotecan, and Irinotecan + GUSi with the same doses as Table S2. However, the frequency of dosing was altered as per Table S4. Animals were closely monitored for diarrhea. Tumor volume, calculated as above with the formula (Length x $Width^2$)/2, and body weight were assessed twice per week; animals losing >20% body weight were euthanized.

C. FVB MICE

Seven-eight week old female FVB/NJ mice were purchased from the Jackson Laboratories, acclimated at UNC for three weeks and then used to perform time-course studies. FVB is the background strain for C3TAg model, and was therefore chosen for time-course and metabolomics studies to minimize the use of costly transgenic mice. Age-, litter- and weight-matched mice were randomized into two cohorts of four groups: vehicle, GUSi, irinotecan, or irinotecan + GUSi (n=3-5 per group), with the same doses and delivery routes described in Table S4. The first cohort was euthanized 24 hours following treatment, and the second cohort was euthanized 120 hours (= five days) after treatment. For metabolomics detection of GUSi, animals were gavaged 1 mg/kg of inhibitor, and euthanized at the indicated time points. For metabolomics detection of SN38 and SN38- G, animals were dosed with 50 mg/kg intraperitoneal irinotecan, with or without concurrent 1mg/kg GUSi by oral gavage; animals were euthanized at the indicated time points. Plasma and luminal contents of small intestine, cecum, and colon were collected into sterile microfuge tubes and snap frozen in liquid nitrogen, transported to Imperial College, London on dry ice, where they were stored at -80°C until subsequent sample preparation.

D. MONOASSOCIATION STUDIES

Germ-free wild-type C57/BL6J mice were bred and maintained in-house at the National Gnotobiotic Rodent Resource Center (NGRRC; University of North Carolina, Chapel Hill, NC). Mice were housed in Green Line

cages (Tecniplast). At 8-10 weeks of age, mice were colonized by oral gavage and rectal swabbing with viable WT *E. coli* MG1655 or the isogenic ΔGUS mutant (15) that were cultured overnight in lysogeny broth in anaerobic conditions, as described above. Colonization was monitored by quantitative plating onto brain heart infusion (BHI) agar plates of serial dilutions of freshly collected feces. Plates were incubated for 24 hours under aerobic conditions at 37°C, and colonies were enumerated. Four weeks following colonization, mice were first weighed, fecal samples collected, and then mice were injected intraperitoneally with 50 mg/kg irinotecan on a schedule illustrated by black arrows in Figure S3E. 24 hours following each injection, all mice were weighed, and fecal samples collected where possible (not possible for a subset of animals due to diarrhea). 24 hours following the second injection, intestinal inflammation was assessed using lipocalin-2 ELISA, and *in fimo* GUS activity using the non-specific substrate 4-MUG. Animals were euthanized 15 days after the first irinotecan injection.

FECAL LIPOCALIN-2 ENZYME-LINKED IMMUNOSORBENT ASSAY (ELISA)

Frozen fecal samples (15-20 mg) were homogenized by vortexing for 1 minute in PBS + 0.1% Tween-20, incubated overnight at 4°C, and subsequently centrifuged at 12,000 x *g* for 10 minutes at 4°C. Clarified supernatants were transferred to fresh tubes, further diluted 500x in assay diluent and ELISA was performed per the manufacturer's (R&D Systems) protocols, with chromogenic detection using a spectrophotometric plate reader.

16S rRNA AMPLICON SEQUENCING

Isolation of total DNA from stool samples was carried out using the MoBio Powerfecal kit per the manufacturer's directions. Total bacterial DNA was amplified using primers targeting the V3-V4 region of the 16S rRNA gene and overhang adapter sequences appended to the primer pair for compatibility with Illumina index and sequencing adapters (16). Master mixes used 2x KAPA HiFi HotStart Ready-mix (KAPA Biosystems, Wilmington, MA). Each 16S rRNA amplicon was purified using AMPure XP reagent (Beckman Coulter, Indianapolis, IN). In the next step each sample was amplified using a limited cycle PCR program, adding Illumina sequencing adapters and optional dual-index barcodes (index 1[i7] and index 2[i5]) (Illumina, San Diego, CA) to the amplicon target. The final libraries were again purified using AMPure XP reagent,

quantified and normalized prior to pooling. The DNA library pool was denatured with NaOH, diluted with hybridization buffer and heat denatured before loading on the MiSeq reagent cartridge and on the MiSeq instrument (Illumina). Automated cluster generation and paired-end sequencing with dual reads was performed.

ANALYSIS OF 16S rRNA SEQUENCES

16S sequencing reads for the athymic mice and C3-tag mice were preprocessed, separately, using QIIME v.1.9.1 (17) with the default parameters except where noted. Briefly, forward and reverse reads were merged, demultiplexed and quality filtered at Q20. One sample from the athymic mice was excluded due to low number of reads. Closed-reference OTUs were picked at 97% similarity level using the Greengenes 97% reference dataset, release 13_8 and taxonomy was assigned using RDP (ribosomal database project) classifier v. 2.2 through QIIME also using Greengenes release 13_8 reference sequences with confidence set to 50%. We excluded OTUs that had ≤0.005% of the total number of sequences according to Bokulich and colleagues (18, 19). PCoA plots were generated from UniFrac (20) after rarefying the counts to the minimum number of reads found in all samples (63,104 for the athymic mice samples and 13,212 for the C3-tag mice samples). Alpha diversity (Chao1 diversity index) was also calculated after rarefying the raw counts to a depth of the minimum count in all samples. We utilized the nlme package v. 3.1-131 in R v. 3.4.3 to analyze the data and account for possible contributions that may arise from co-housing groups of mice in the same cage (21). We built two models one with cage modeled as a random effect and treatment or group as fixed effects and one without cage. We then used ANOVA to compare the two models and the resulting P-value (calculated using F-test) was used to determine the effect of co-housing. The treatment or group P-values were calculated using ANOVA on the mode that doesn't include cage. We controlled for false discovery rate (FDR) by correcting the P-values using the Benjamini and Hochberg (BH) approach (22). The submission ID for the NCBI SRA is SUB4783842, and the BioProject ID is PRJNA505302.

HISTOPATHOLOGICAL ANALYSES AND CLINICAL SCORING SCHEMES

All histopathological scoring was performed on slides obscured of any identifying marks and verified by a Board-certified veterinary pathologist (SAM). Quantification of apoptotic and proliferating cells was performed

in comparable segments of large and small intestine across all samples. Ten consecutive, well-formed crypts were quantified from all regions. Rounded cells with condensed, strongly hematoxylin stained nuclei were counted as apoptotic. Colon histopathology was quantified based on the grading scheme described by Cooper *et al. (23)*, and evaluated for three parameters described below: infiltrating inflammatory cells, crypt damage, and regeneration, each of which are described in detail below:

Infiltrating inflammatory cells

0: Normal

1: Small leukocyte aggregates in mucosa and/or submucosa

2: Coalescing mucosal and/or submucosal inflammation

3: Coalescing mucosal inflammation with prominent multifocal submucosal extension +/- follicle formation

4: Severe diffuse inflammation of mucosa, submucosa, & deeper layers

Inflammation was graded on the above subjective scale, and multiplied with the extent score from Table S5 to arrive at an inflammation score.

Crypt damage

0 None

1 Basal 1/3 damaged

2 Basal 2/3 damaged

3 Only surface epithelium intact

4 Entire crypt and epithelium lost

Crypt damage was assessed based on the pathologic changes described above, then multiplied by the extent score from Table S7. This product was considered as the total crypt damage score.

Regeneration

4 No evidence of repair

3 Early attempts at regeneration i.e., plump crypts.

2 More mature regenerative crypts

1 Minimal crypt depletion

0 Complete regeneration or normal tissue

Regeneration was assessed based on the pathologic changes described above, and multiplied by the extent score from Table S5. This product was considered as the total regeneration score.

STATISTICAL ANALYSES

Detailed statistical analyses for each figure are presented in Table S6. All analyses were performed using Graphpad Prism v6, except for Figure 5, which was analyzed using R v. 3.4.3.

Data Availability Statement: All data discussed in the paper will be made available to readers.

Table S1: Data collection and refinement statistics.

Resolution	48.7 – 2.69
(highest shell: Å)	2.73 – 2.69
Space group	$C222_1$
Unit cell dimensions (a,b,c: Å)	71.3, 292, 240.5
Total reflections (F>0)	327,990
Unique reflections	69,571
Multiplicity	4.7 (4.8)
Completeness, %(highest shell)	98.8 (99.7)
Mean I/sigma (I) (highest shell)	11.1 (1.8)
R_{work} (highest shell)	0.195 (0.284)
R_{free} (highest shell)	0.230 (0.327)
Number of water molecules in asymmetric unit	354
rms bonds (Å)	0.005
rms angles (°)	1.2
Ramachandran favored (%)	94
Ramachandran outliers (%)	0.8
Average B-factor ($Å^2$)	50.9
RCSB ID	6CXS

Table S2:

Group	Dose and route of delivery	Frequency
Control	Vehicle	Every weekday
GUSi	10 ug by oral gavage, total dose 20 ug daily as previously reported(9, 10).	Twice daily on weekdays
Irinotecan	50 mg/kg by intraperitoneal injection	Every weekday
GUSi + irinotecan	GUSi: 10 ug by oral gavage, total dose 20 ug daily Irinotecan: 50 mg/kg by intraperitoneal injection	GUSi: twice daily on weekdays Irinotecan: Every weekday

Table S3: List of primers and probes used to genotype C3TAg mice

Primer	Sequence
C3TAg Forward	5'-GGT AAA CAT ATG ACT TGG GTT C-3'
C3TAg Reverse	5'-TGA GAC CTC AGT GTT CCT CT-3'
C3TAg gene probe	5'- (FAM) CTC AGG CAA TCA CCT TAG TCT TGC CC (TAMRA)
Endogenous Forward	5'-TCG TTC ACC GTG TAT GCT TC-3'
Endogenous Reverse	5'-CAG CAG GCC ACA TGC TGT T-3'
Endogenous Probe	5'-(JOE) TG TCC TCG TAG GCA CAC AAT ATG CAG ACA (TAMRA)

Table S4: Dosing schedule for C3TAg mice.

Week #	Dose frequency
1	Twice weekly
2	Thrice weekly
3	Thrice weekly
4, 5, 6...	Daily (weekdays)

Table S5: Extent score and percentage involvement scheme.

Extent score	Percentage involvement
1	1-25%
2	26-50%
3	51-75%
4	76-100%

Table S6: Description of statistical tests used in figures in the main body of text. Included are figure numbers (Column 1), statistical test and post-hoc tests (if any) in Column 2, the F(DFn, DFd) and t statistical values in Column 3, and the *P* value in Column 4.

Figure	Test	Statistics	*P* value
1B	Two-way ANOVA	Treatment; $F_{(2,54)} = 62.22$	<0.0001
		Group; $F_{(8,54)} = 27.72$	<0.0001
		Treatment x Group; $F_{(16,554)} = 8.466$	<0.0001
	Tukey's multiple comparisons test	*Ec*GUS: control vs GUSi-Inh1	<0.0001
		Control vs GUSi-UNC10201652	<0.0001
		*Ee*GUS: control vs GUSi-Inh1	<0.0001
		Control vs GUSi-UNC10201652	<0.0001
		Inh1 vs UNC10201652	0.0016
		*Sa*GUS: control vs GUSi-Inh1	0.0002
		Control vs GUSi-UNC10201652	<0.0001
		Inh1 vs UNC10201652	0.0003
		*Cp*GUS: control vs GUSi-Inh1	ns
		Control vs GUSi-UNC10201652	0.0009
		Inh1 vs UNC10201652	0.0206
		*Bf*GUS: control vs GUSi-Inh1	0.1294
		Control vs GUSi-UNC10201652	0.0101
		Inh1 vs UNC10201652	0.5376

		*Bu*GUS: control vs GUSi-Inh1	0.7325
		Control vs GUSi-UNC10201652	0.7112
		Inh1 vs UNC10201652	0.9993
		*Pm*GUS: control vs GUSi-Inh1	>0.99
		Control vs GUSi-UNC10201652	>0.99
		Inh1 vs UNC10201652	>0.99
		*Bo*GUS: control vs GUSi-Inh1	0.8783
		Control vs GUSi-UNC10201652	0.8240
		*Bd*GUS: control vs GUSi-Inh1	0.9947
		Control vs GUSi-UNC10201652	>0.9999
		Inh1 vs UNC10201652	0.999
1C	One-way ANOVA	Treatment; F(3,11) = 8.245	0.0037
	Sidak's multiple comparisons test	Control vs GUSi	0.8859
		Control vs IRI	0.0359
		Control vs IRI + GUSi	>0.9999
		Irinotecan vs IRI + GUSi	0.0190
		GUSi vs IRI + GUSi	0.8848
2A	One-way ANOVA	Treatment; F(3,11) = 7.395	0.0055
	Sidak's multiple comparisons test	Vehicle vs. GUSi	0.9435
		Vehicle vs. IRI	0.0051
		Vehicle vs. IRI + GUSi	0.3721
		IRI vs IRI + GUSi	0.0484
2B	One-way ANOVA	Treatment; F(3,14) = 10.64	0.0007
	Sidak's multiple comparisons test	Vehicle vs. GUSi	0.8016
		Vehicle vs. IRI	0.0008
		Vehicle vs. IRI + GUSi	0.0148
2C	One-way ANOVA	Treatment; F(3,20) = 6.837	0.0024
	Sidak's multiple comparisons test	Vehicle vs. GUSi	0.0536
		Vehicle vs. IRI	0.0012
		Vehicle vs. IRI + GUSi	0.4729
		IRI vs. IRI + GUSi	0.0381
3A	Log-rank (Mantel-Cox) test	Chi^2 = 6.606, df = 1	0.0102
3B	One-way ANOVA	F(3,20) = 11.69	0.0001
	Sidak's multiple comparisons test	Vehicle vs. IRI	0.0005
		Vehicle vs. IRI + GUSi	0.0009
		IRI vs. IRI + GUSi	0.9998
4A	Log-rank (Mantel-Cox) test	Chi^2 = 4.962, df = 1	0.059

4B	One-way ANOVA	Treatment: F(3,27) = 7.656	0.0007
	Sidak's multiple comparisons test	Vehicle vs. GUSi	>0.9999
		Vehicle vs. IRI	0.3543
		Vehicle vs. IRI + GUSi	0.0093
		IRI vs. IRI + GUSi	0.4006
5A	One-way ANOVA	IRI Group vs. noIRI Group: F(1,20) = 10.42	0.004
		irinotecan vs. GUSi treatment: F(1,10) = 8.67	0.01
		irinotecan and vehicle treatment: F(1,10) = 12.30	0.005
5B	One-way ANOVA	IRI Group vs. noIRI Group: F(1,20) = 11.35	0.003
		vehicle vs. irinotecan treatment: F(1,10) = 7.38	0.022
		irinotecan vs. GUSi treatment: F(1,10) = 10.25	0.009
5C	One-way ANOVA	IRI Group vs. noIRI Group: F(1,30) = 26.54	0.0003
5D	One-way ANOVA	IRI Group vs. noIRI Group: F(1,30) = 17.7	0.0008
Supp. Fig 2A	Two-way ANOVA	Mouse; $F_{(2,9)}$ = 1252	
		Treatment; $F_{(2,9)}$ = 30.03	
		Treatment x mouse; $F_{(4,9)}$ = 8.801	0.0036
			<0.0001
	Sidak's multiple comparisons test	Mouse #1: control vs. Inh1	0.0001
		Control vs. UNC10201652	0.0355
		Mouse #2: control vs. Inh1	<0.0001
		Control vs. UNC10201652	0.3781
		Mouse #3: control vs. Inh1	0.0073
		Control vs. UNC10201652	ns
			ns
Supp Fig 2B	Two-way ANOVA	Mouse; $F_{(2,18)}$ = 269.4	<0.0001
		Treatment; $F_{(2,18)}$ = 27.22	<0.0001
		Treatment x Group; $F_{(4,18)}$ = 7.229	0.0012
	Sidak's multiple comparisons test	Mouse #1: control vs. Inh1	0.5485
		Control vs. UNC10201652	0.0003
		Mouse #2: control vs. Inh1	<0.0001

		Control vs. UNC10201652	<0.0001
		Mouse #3: control vs. Inh1	0.9137
		Control vs. UNC10201652	0.5144
Supp Fig 2C	Two-way ANOVA	Mouse; $F_{(2,18)} = 560.8$	<0.0001
		Treatment; $F_{(2,18)} = 36.38$	<0.0001
		Treatment x Group; $F_{(4,18)} = 1.748$	0.1834
	Dunnett's multiple comparisons test	Mouse #1: control vs. Inh1	0.217
		Control vs. UNC10201652	<0.0001
		Mouse #2: control vs. Inh1	0.3632
		Control vs. UNC10201652	0.0129
		Mouse #3: control vs. Inh1	0.6269
		Control vs. UNC10201652	0.0003
Supp Fig 3D	Unpaired t test	Two-tailed t= 2.378, df=12	0.0349
Supp Fig 6A	One-way ANOVA	Treatment; F(3,28) = .74	<0.0001
	Sidak's multiple comparisons test	Vehicle vs. GUSi	>0.9999
		Vehicle vs. IRI	0.0002
		Vehicle vs. IRI + GUSi	0.2076
		IRI vs. IRI + GUSi	0.0004
Supp Fig 6B	One-way ANOVA	F(3,15)=11.07	0.0004
		Vehicle vs GUSi	0.1303
	Dunnett's multiple comparisons test	Vehicle vs IRI	0.0009
		Vehicle vs IRI + GUSi	0.0005
Supp Fig 8B	Long-rank (Mantel-Cox) test	Chi^2=10.09, df = 3	0.0178

Supp Fig 8E	Savitsky-Golay smoothing	Second order with four neighbors, with no differentiation or integration performed.	
	Ordinary one-way ANOVA Sidak's multiple comparisons test	Treatment: F(3,76)	<0.0001
		Vehicle vs GUSi	0.7081
		Vehicle vs IRI	0.0168
		Vehicle vs IRI + GUSi	0.0006
		IRI vs IRI + GUSi	0.8144
Supp Fig 9A	One-way ANOVA	IRI group vs noIRI group: F(1, 20)=22.02	0.0001
Supp Fig 9B	One-way ANOVA	IRI group vs noIRI group: F(1, 30)=8.28	0.007

SUPPLEMENTAL FIGURES

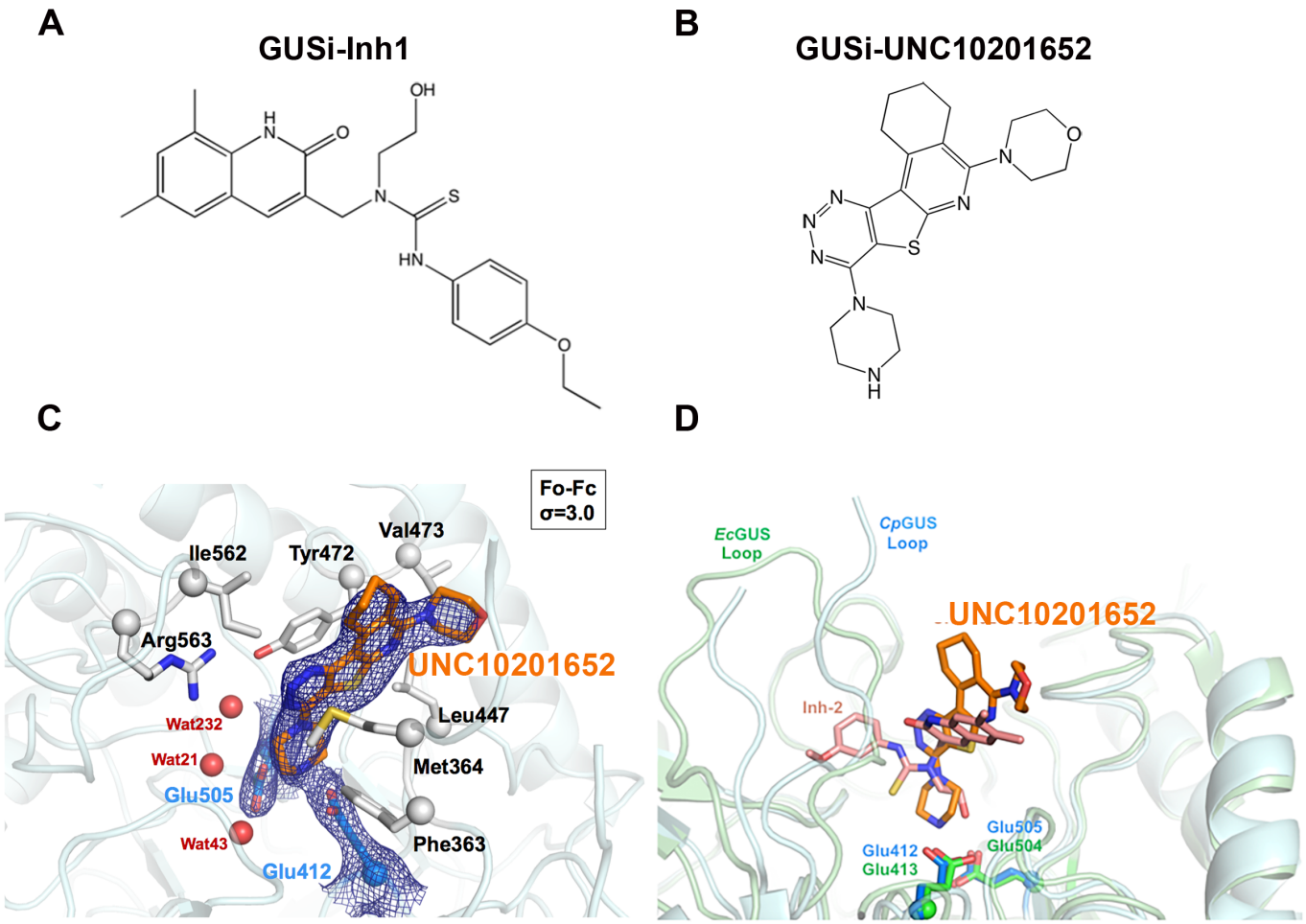

Supplemental Figure 1: GUSi inhibit microbial ß-glucuronidase via binding the catalytic active site.

(A) Structure of bacterial ß-glucuronidase inhibitor (GUSi) termed “Inhibitor 1” previously reported by Wallace *et al. (1)*. **(B)** Structure of GUSi compound **UNC10201652**, which contains a piperazine moiety. **(C)** Active site residues surround the bound **UNC10201652** (orange) in the *Cp*GUS crystal structure. A Fo-Fc omit map (σ=3.0) is shown on **UNC10201652** and the adjacent catalytic glutamic acid residues (blue). **(D)** Structural active site superposition of the **UNC10201652**-bound *Cp*GUS (light blue) and Inh2-bound *Ec*GUS (light green) crystal structures. **UNC10201652** (orange) and Inh2 (*1*) (pink) are shown adjacent to the conserved catalytic glutamic acids. The nitrogen in the piperazine group of Inh9 is positioned similarly to the hydroxyethyl group of Inh2, indicating a common need for a

proton donor/acceptor group near the catalytic Glu412/Glu413. The polypeptide Loop 1 regions common to this clade of bacterial GUS enzymes contact the inhibitors and are labeled.

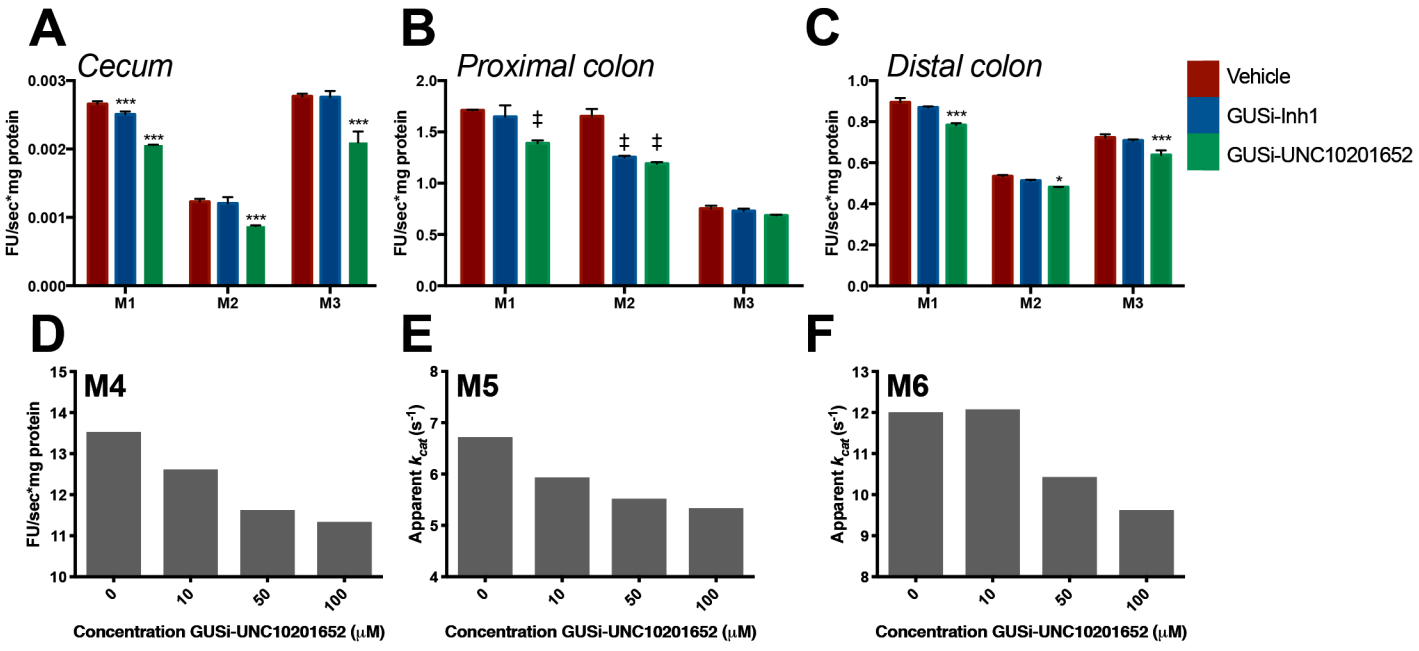

Supplemental Figure 2:

Variable GUS catalytic activity towards SN38-G is observed *in fimo* from luminal contents isolated from **(A)** cecum **(B)** proximal and **(C)** distal colon in three wild-type FVB mice (M1, M2, M3) sourced from three different cages. GUSi diminishes the *in fimo* GUS activities measured to varying degrees, but in nearly all cases in a manner that is statistically significant. Error bars are ±SEM, ‡ P <0.0001, *** P <0.001, * P <0.05 by two-way ANOVA with Dunnett's multiple comparisons test. GUSi-**UNC10201652** reduces *in fimo* GUS activity with SN38-G from cecal contents in a dose-dependent manner, as shown in **(D)-(F).** Initial velocities values for three different wild-type FVB mice (M4, M5, M6) sourced from different cages with increasing amounts of GUSi-**UNC10201652** are plotted. All data are normalized to total fecal protein content. FU = fluorescence units.

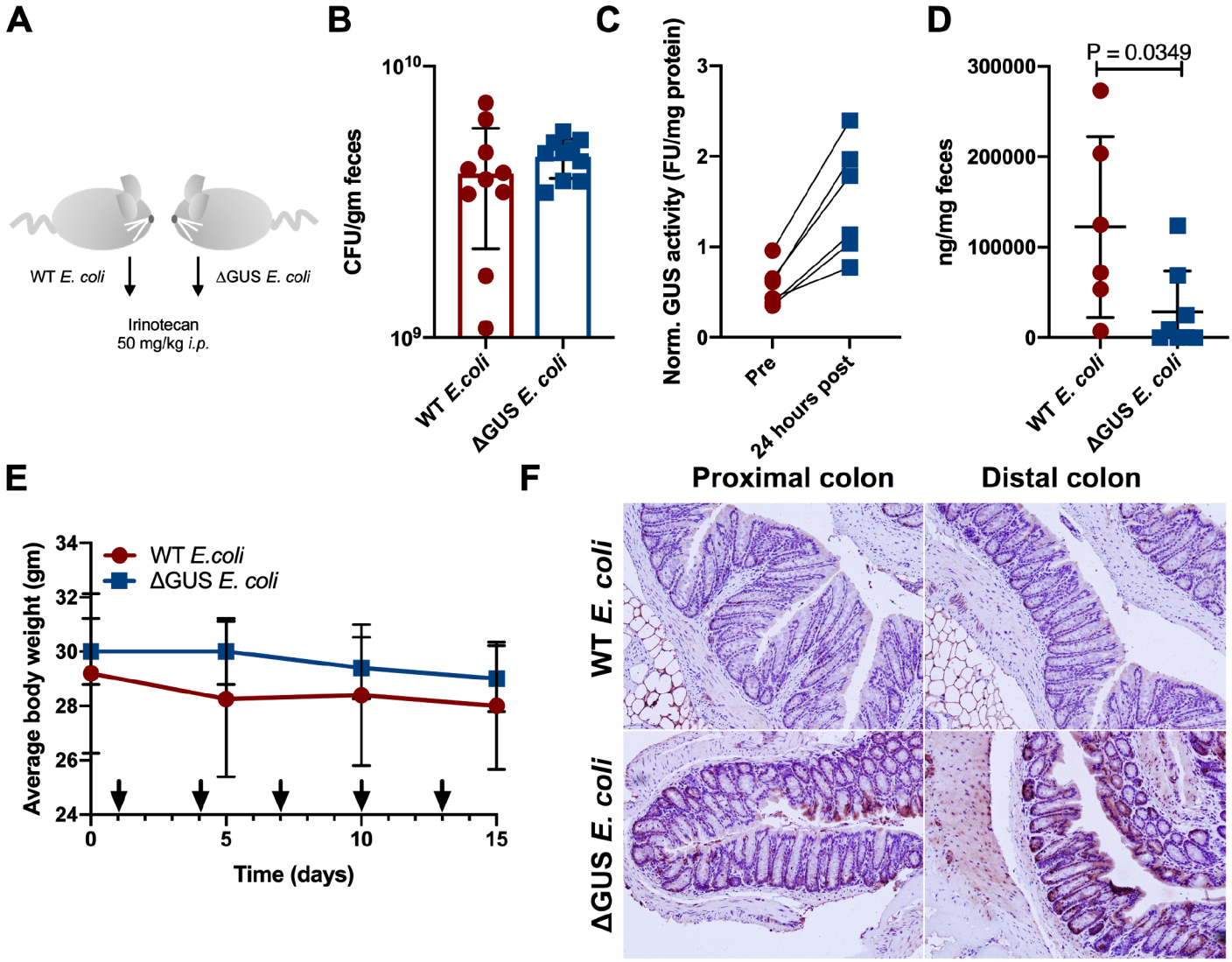

Supplemental Figure 3: Irinotecan reduces proliferation and increases intestinal inflammation in a GUS-dependent manner. (A) Germ-free wild-type mice were colonized with either WT or ΔGUS *E. coli* MG1655, confirmed by **(B)** plating onto BHI agar plates. In WT *E. coli* mono-associated mice, a single dose of irinotecan increased **(C)** GUS activity, and **(D)** intestinal inflammation as quantified by fecal lipocalin-2. **(E)** Modest changes in body weight with irinotecan dosing (on days indicated by black arrows) translated into a stark reduction in **(F)** colonic epithelial proliferation as assessed by BrdU immunohistochemistry in WT *E. coli* colonized mice. In contrast, ΔGUS *E. coli* colonized animals displayed **(D)** lower fecal lipocalin-2 and **(F)** healthy colon epithelial cell proliferation.

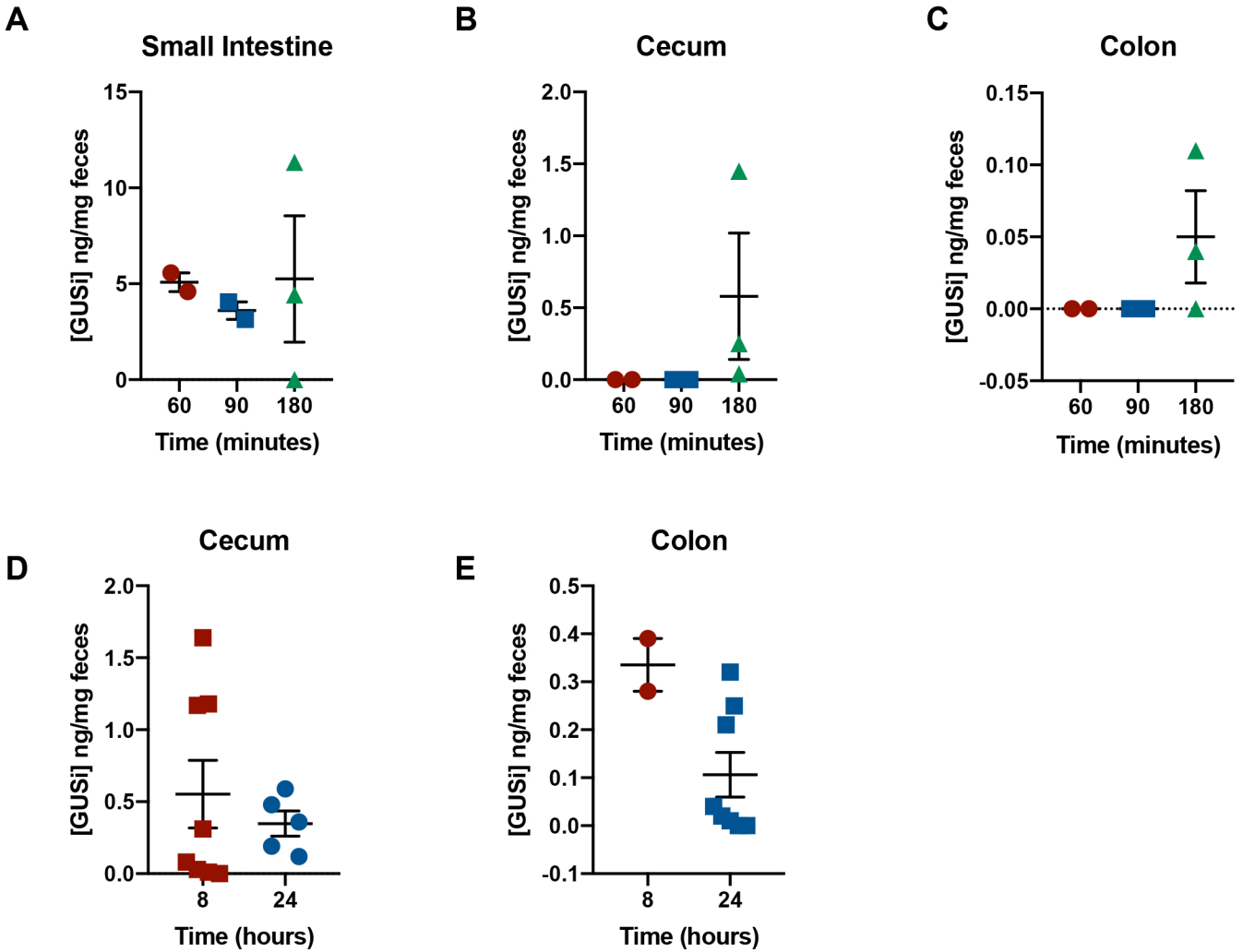

Supplemental Figure 4: Orally-dosed 1 mg/kg GUSi reaches the murine gastrointestinal tract. It is detected anteriorly in the **(A)** small intestine within 60 minutes. After 180 minutes it is detectable in the cecum and colon **(B, C** respectively**)**. Importantly, GUSi remains detectable in the **(D)** cecum and **(E)** colon after eight and up to 24 hours following dosing. Quantified GUSi is normalized to the total intraluminal fecal content. In panel E, only two mice had sufficient colon contents at eight hours for use in mass spectrometry analysis.

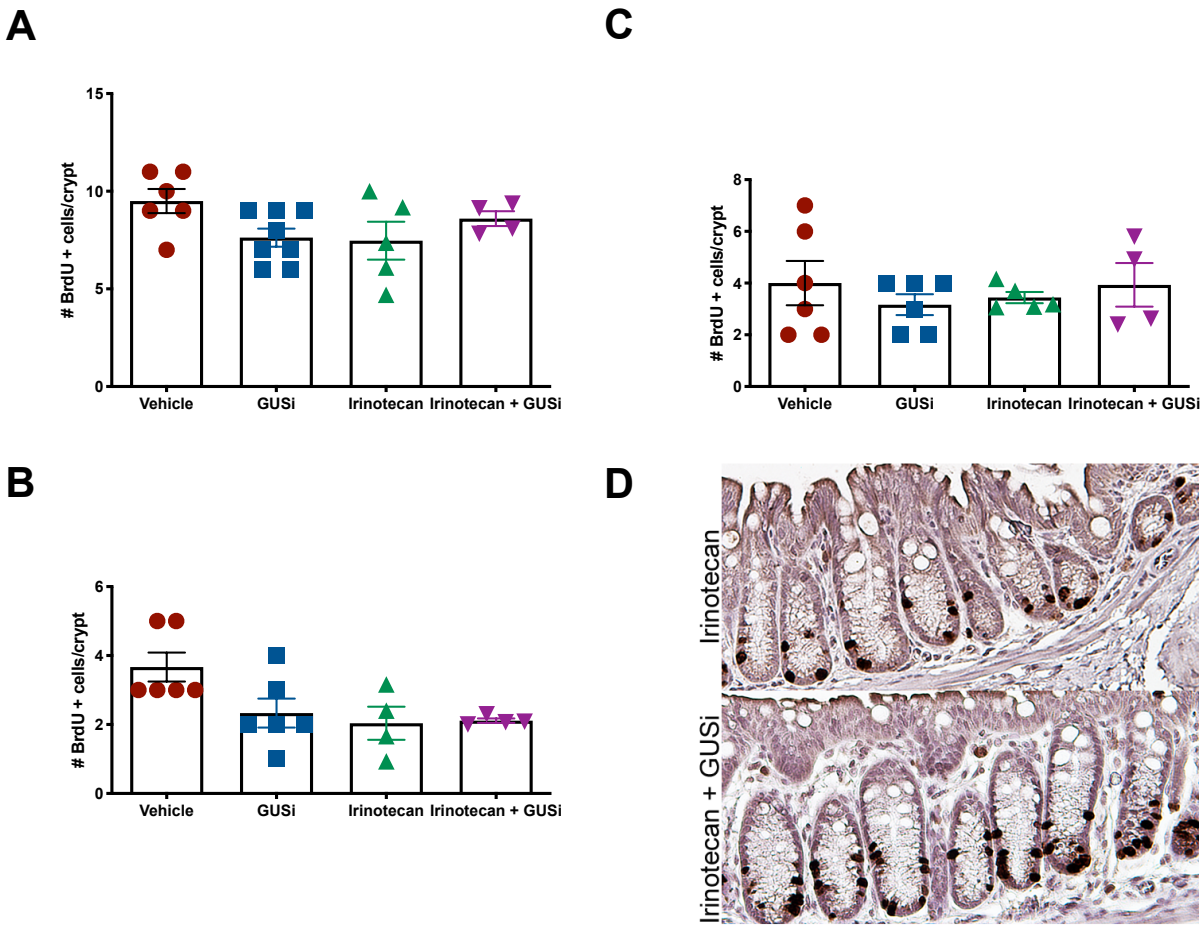

Supplemental Figure 5: GUSi modestly reduces the acute toxicity 24 hours after single IRI injection. Mice were injected with BrdU for 30 min prior to euthanasia to assess proliferating intestinal cells. The numbers of BrdU+ cells in ten consecutive crypts were blindly quantified in the **(A)** ileum **(B** proximal colon **(C)** distal colon; no differences were observed. **(D)** Immunohistochemistry to detect BrdU+ cells (*brown*) in distal colons of mice treated as indicated; nuclei are counterstained with hematoxylin (*blue*).

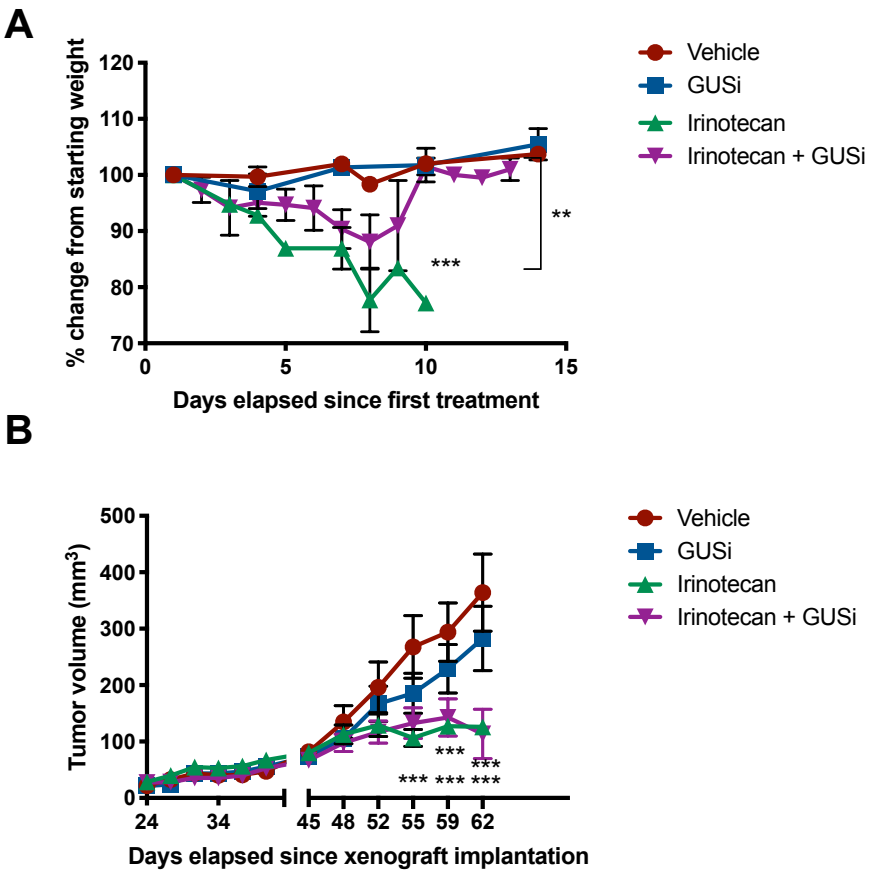

Supplemental Figure 6: (A) Percent change in body weight of athymic nude mice bearing Sum149 xenografts throughout treatment course. $^{**}P < 0.01$, $^{***}P < 0.001$ by one-way ANOVA (Sidak multiple comparison test). No significant changes were observed in dual-treated mice compared to controls. **(B)** GUSi cotreatment results in significant tumor regression to levels similar to single agent irinotecan. $^{***}P < 0.001$ by one-way ANOVA (Dunnett multiple comparison test to vehicle treatment).

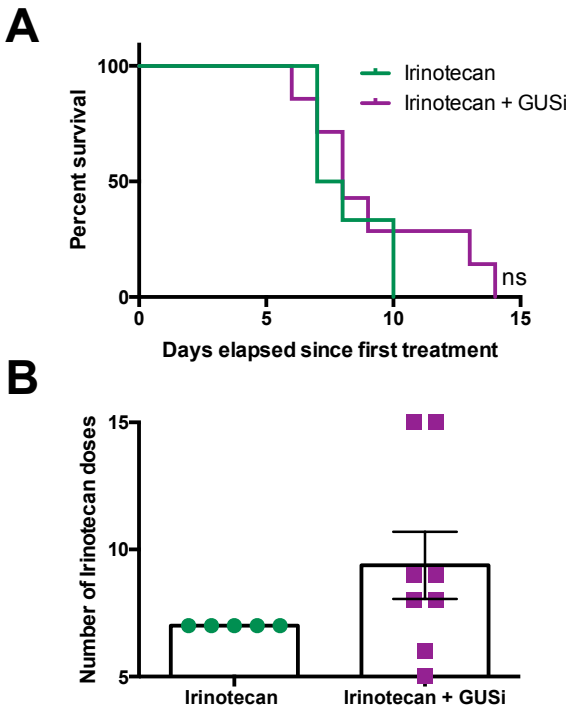

Supplemental Figure 7:

(A) IRI + GUSi treated athymic nude mice exhibit a trend towards slightly improved overall survival compared to IRI treatment alone, although not statistically significant; ns, not significant. **(B)** Co-treatment with GUSi allows athymic nude mice to tolerate higher number of IRI doses, compared to IRI treatment alone.

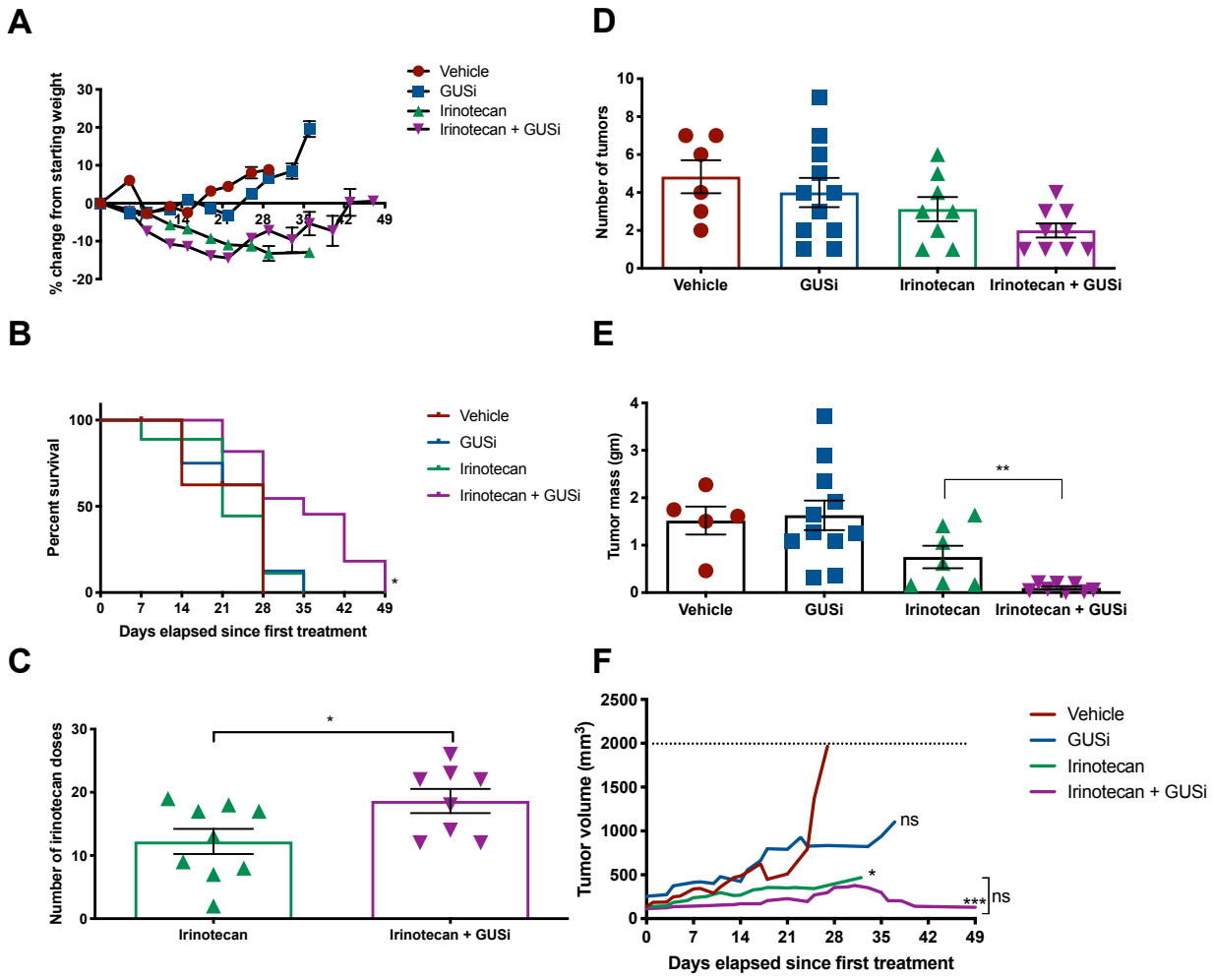

Supplemental Figure 8: (A) Percent change in body weight of C3TAg GEMM mice throughout treatment course. § single animal remaining at this time point. **(B)** GUSi co-treatment extends the overall survival of irinotecan-treated mice by 14 days. *P< 0.05 by Log-Rank (Mantel-Cox) test. **(C)** With GUSi co-treatment, IRI-treated mice tolerate a significantly higher number of IRI doses compared to IRI alone. *P< 0.05 by one-way ANOVA with Dunnett's correction for multiple comparisons. **(D)** Regardless of treatment, C3TAg mice have similar number of tumors upon initiation of treatment. Tumor number reflects the primary tumor as well as at secondary sites as previously reported by Green, *et al.* **(E)** Irinotecan reduces tumor masses in C3TAg animals,

compared to vehicle or GUSi treatment. IRI + GUSi significantly diminishes tumor masses compared to irinotecan alone. ** $P < 0.01$ by one-way ANOVA with Sidak's multiple comparisons test. **(F)** Smoothed curves of tumor volumes (statistical methods described in *Supplemental Information)* indicate that compared to vehicle or GUSi alone, irinotecan and irinotecan + GUSi significantly (* $P < 0.05$, *** $P < 0.001$ respectively by one-way ANOVA with Sidak's multiple comparisons test) reduce tumor volumes. Regression analysis reveals no significant differences in tumor volumes between irinotecan and irinotecan + GUSi, confirming that GUSi cotreatment does not affect the antitumor activity of irinotecan.

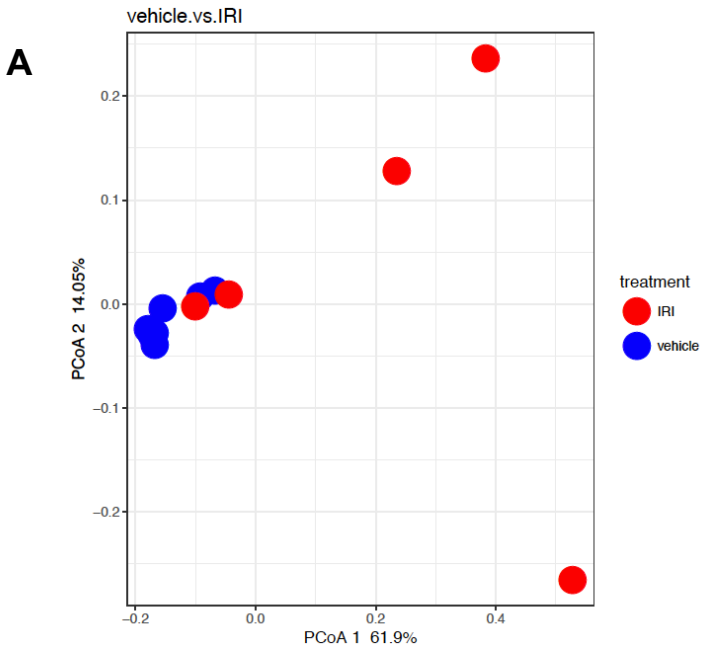

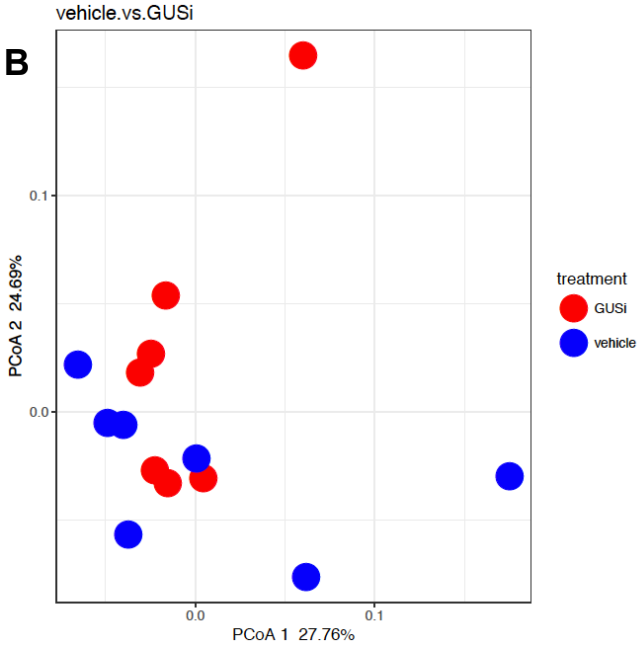

	P value	Cage P value		P value	Cage P value
Axis.1	0.007313631	0.324247272	Axis.1	0.713269387	0.974581545
Axis.2	0.616783211	0.019386312	Axis.2	0.117505486	0.107451808

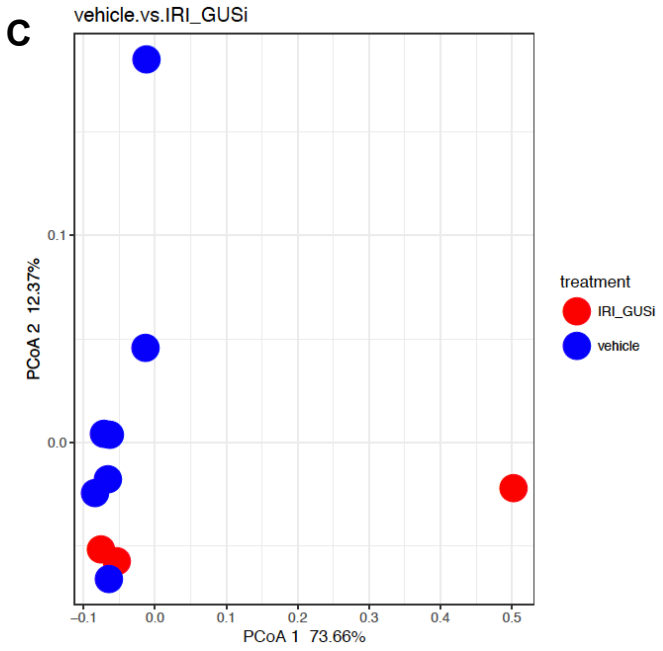

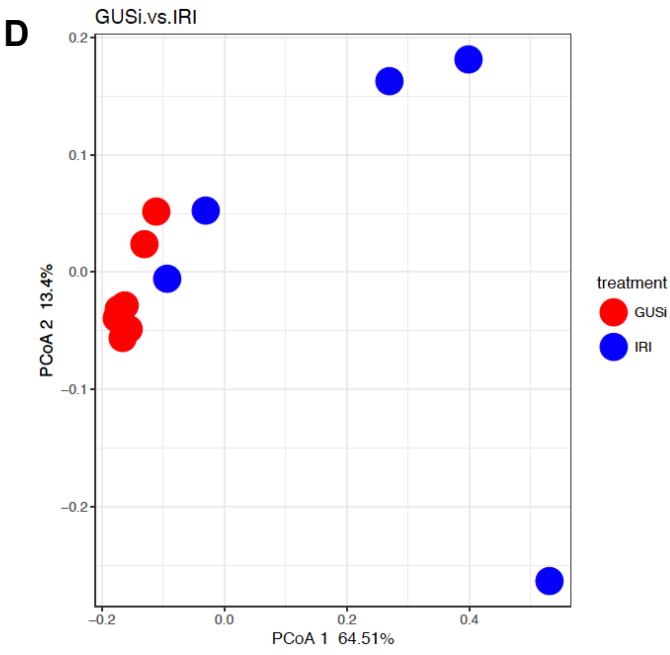

	P value	Cage P value		P value	Cage P value
Axis.1	0.157905355	0.988872536	Axis.1	0.004346672	0.439129776
Axis.2	0.237778999	0.978737924	Axis.2	0.540431448	0.00715239

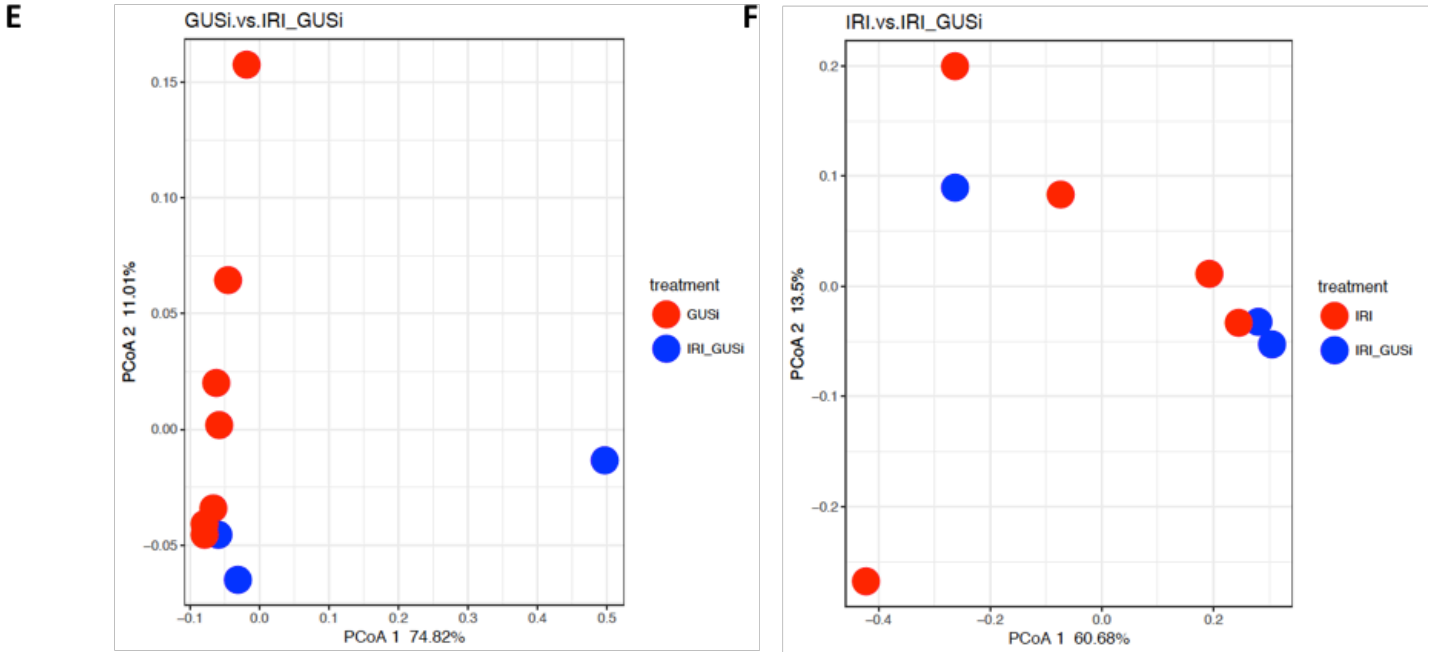

	P value	Cage P value		P value	Cage P value
Axis.1	0.113115637	0.988796297	Axis.1	0.461322633	0.596201951
Axis.2	0.222686756	0.092246154	Axis.2	0.977112807	0.068961183

Supplemental Figure 9: Gut microbial composition of athymic mice bearing Sum149 triple-negative breast cancer xenograft is affected by irinotecan. Principal coordinates analysis showing pairwise comparisons between the four treatments. P values for texting the null hypothesis that treatment didn't change microbial composition and the change is not due to co-housing (cage) are shown below each plot. Comparisons made for each panel are indicated. **(A)** Vehicle vs. IRI **(B)** Vehicle vs. GUSi **(C)** Vehicle vs. IRI+GUSi **(D)** GUSi vs. IRI **(E)** GUSi vs. IRI+GUSi **(F)** IRI vs. IRI+GUSi.

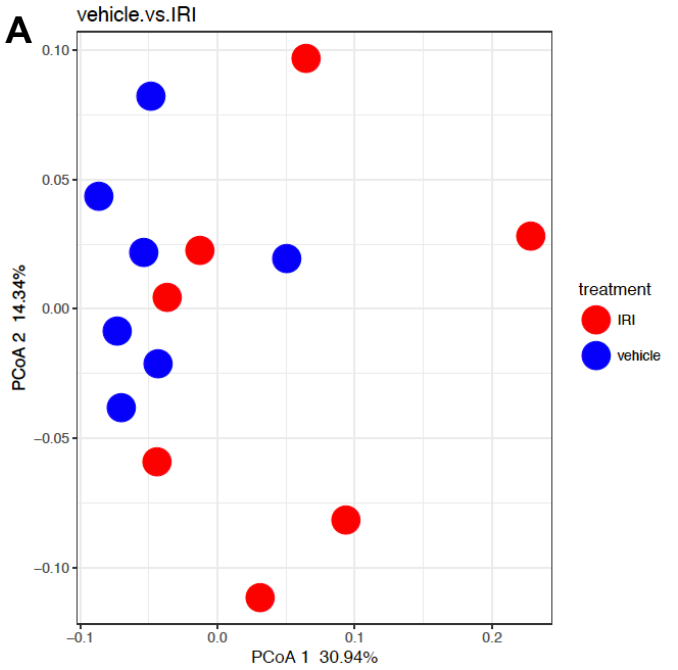

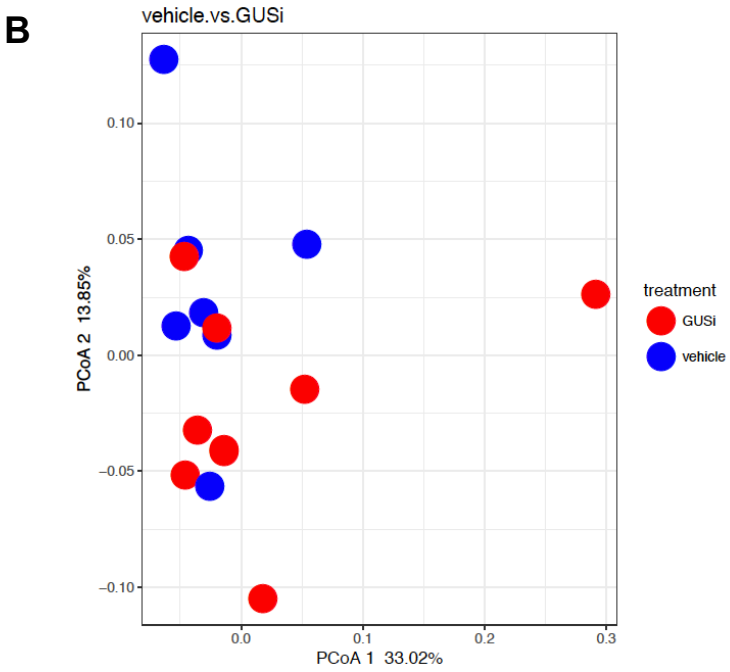

	P value	Cage P value		P value	Cage P value
Axis.1	0.037744897	0.561216315	Axis.1	0.290154882	0.985650951
Axis.2	0.385051039	0.012233194	Axis.2	0.057681869	0.986008803

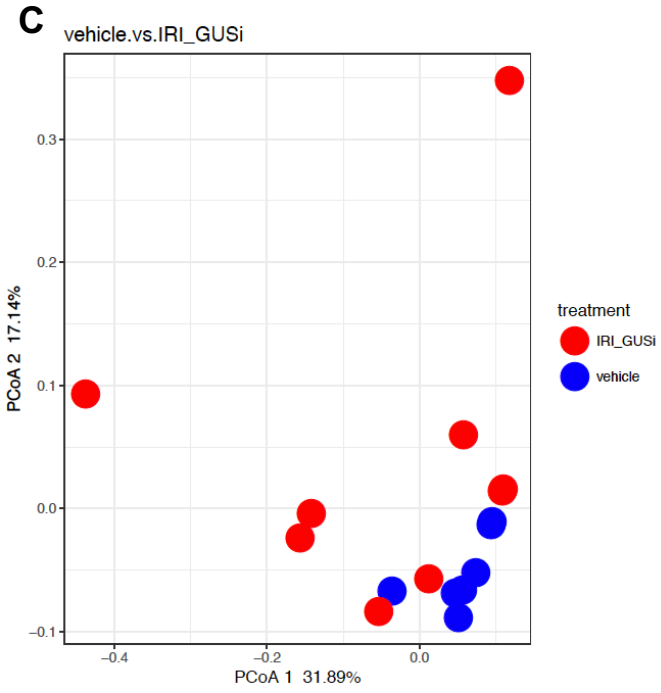

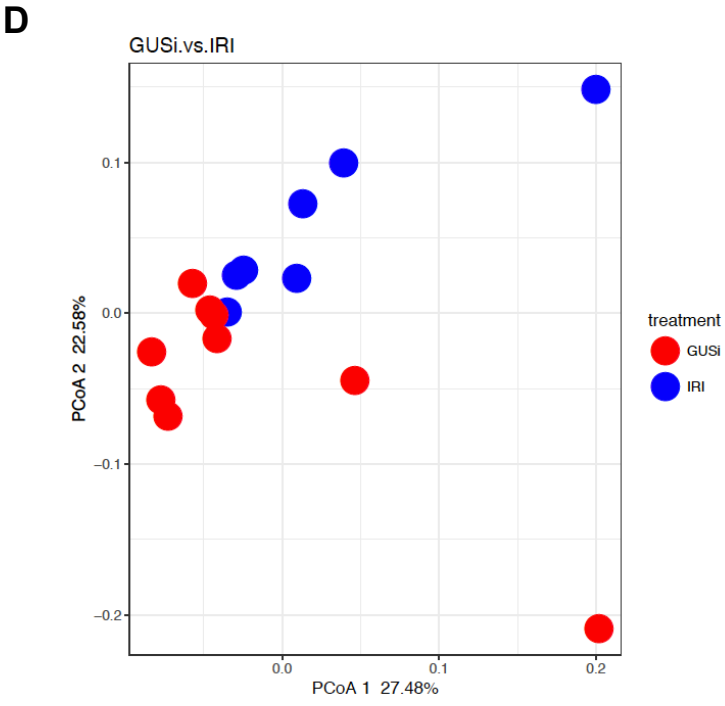

	P value	Cage P value		P value	Cage P value
Axis.1	0.191261987	0.416708501	Axis.1	0.335745806	0.986372111
Axis.2	0.08226328	0.985417056	Axis.2	0.005847401	0.985909973

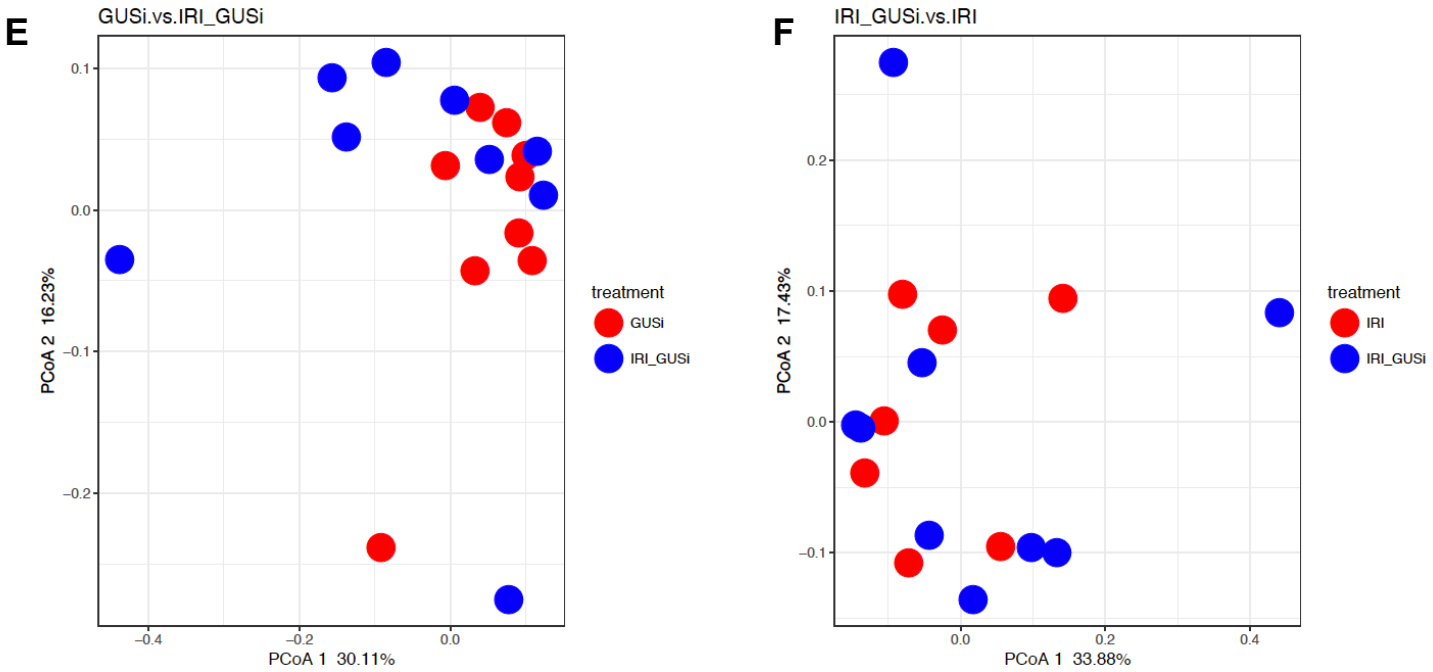

	P value	Cage P value		P value	Cage P value
Axis.1	0.141638946	0.514936154	Axis.1	0.488156568	0.376476121
Axis.2	0.644090694	0.98592769	Axis.2	0.926847125	0.985690936

Supplemental Figure 10. Gut microbial composition of C3Tag mice is affected by irinotecan as revealed by principal coordinates analysis showing pairwise comparisons between the four treatments. P values for testing the null hypothesis that treatment did not change microbial composition and the change is not due to co-housing (cage) are shown below each plot. Comparisons made for each panel are indicated. **(A)** Vehicle vs. IRI **(B)** Vehicle vs. GUSi **(C)** Vehicle vs. IRI+GUSi **(D)** GUSi vs. IRI **(E)** GUSi vs. IRI+GUSi **(F)** IRI+GUSi vs. IRI.

SUPPLEMENTAL REFERENCES

1. B. D. Wallace *et al.*, Alleviating cancer drug toxicity by inhibiting a bacterial enzyme. *Science* **330**, 831-835 (2010).
2. A. J. McCoy *et al.*, Phaser crystallographic software. *J Appl Crystallogr* **40**, 658-674 (2007).
3. P. Emsley, K. Cowtan, Coot: model-building tools for molecular graphics. *Acta Crystallogr D Biol Crystallogr* **60**, 2126-2132 (2004).
4. N. W. Moriarty, R. W. Grosse-Kunstleve, P. D. Adams, electronic Ligand Builder and Optimization Workbench (eLBOW): a tool for ligand coordinate and restraint generation. *Acta Crystallogr D Biol Crystallogr* **65**, 1074-1080 (2009).
5. S. J. Pellock *et al.*, Gut Microbial beta-Glucuronidase Inhibition via Catalytic Cycle Interception. *ACS Cent Sci* **4**, 868-879 (2018).
6. M. S. Little, S. J. Pellock, W. G. Walton, A. Tripathy, M. R. Redinbo, Structural basis for the regulation of beta-glucuronidase expression by human gut Enterobacteriaceae. *Proc Natl Acad Sci U S A* **115**, E152-E161 (2018).
7. A. P. Bhatt, L. Grillo, M. R. Redinbo, In Fimo: A Term Proposed for Excrement Examined Experimentally. *Gastroenterology* **156**, 1232 (2019).
8. S. Ohdo *et al.*, Cell cycle-dependent chronotoxicity of irinotecan hydrochloride in mice. *J Pharmacol Exp Ther* **283**, 1383-1388 (1997).
9. B. D. Wallace *et al.*, Structure and Inhibition of Microbiome beta-Glucuronidases Essential to the Alleviation of Cancer Drug Toxicity. *Chem Biol* **22**, 1238-1249 (2015).
10. B. D. Wallace *et al.*, Alleviating cancer drug toxicity by inhibiting a bacterial enzyme. *Science* **330**, 831-835 (2010).
11. J. C. Arthur *et al.*, Intestinal inflammation targets cancer-inducing activity of the microbiota. *Science* **338**, 120-123 (2012).
12. A. P. Bhatt *et al.*, Dual inhibition of PI3K and mTOR inhibits autocrine and paracrine proliferative loops in PI3K/Akt/mTOR-addicted lymphomas. *Blood* **115**, 4455-4463 (2010).
13. J. E. Green *et al.*, The C3(1)/SV40 T-antigen transgenic mouse model of mammary cancer: ductal epithelial cell targeting with multistage progression to carcinoma. *Oncogene* **19**, 1020-1027 (2000).
14. P. J. Roberts *et al.*, Combined PI3K/mTOR and MEK inhibition provides broad antitumor activity in faithful murine cancer models. *Clin Cancer Res* **18**, 5290-5303 (2012).
15. K. A. Biernat *et al.*, Structure, function, and inhibition of drug reactivating human gut microbial beta-glucuronidases. *Sci Rep* **9**, 825 (2019).
16. A. K. Bartram, M. D. Lynch, J. C. Stearns, G. Moreno-Hagelsieb, J. D. Neufeld, Generation of multimillion-sequence 16S rRNA gene libraries from complex microbial communities by assembling paired-end illumina reads. *Appl Environ Microbiol* **77**, 3846-3852 (2011).
17. J. G. Caporaso *et al.*, QIIME allows analysis of high-throughput community sequencing data. *Nature methods* **7**, 335-336 (2010).
18. N. A. Bokulich, D. A. Mills, Improved selection of internal transcribed spacer-specific primers enables quantitative, ultra-high-throughput profiling of fungal communities. *Appl Environ Microbiol* **79**, 2519-2526 (2013).
19. N. A. Bokulich *et al.*, Quality-filtering vastly improves diversity estimates from Illumina amplicon sequencing. *Nature methods* **10**, 57-59 (2013).
20. C. Lozupone, M. Hamady, R. Knight, UniFrac--an online tool for comparing microbial community diversity in a phylogenetic context. *BMC Bioinformatics* **7**, 371 (2006).
21. J. McCafferty *et al.*, Stochastic changes over time and not founder effects drive cage effects in microbial community assembly in a mouse model. *ISME J* **7**, 2116-2125 (2013).

22. Y. Benjamini, & Hochberg, Y., Controlling the False Discovery Rate: A Practical and Powerful Approach to Multiple Testing. *Journal of the Royal Statistical Society. Series B (Methodological)* **57**, 289-300 (1995).
23. H. S. Cooper, S. N. Murthy, R. S. Shah, D. J. Sedergran, Clinicopathologic study of dextran sulfate sodium experimental murine colitis. *Lab Invest* **69**, 238-249 (1993).